Volume 28
Number 8
23 February 2026
Pages 3357-3900

Green Chemistry

Cutting-edge research for a greener sustainable future

rsc.li/greenchem

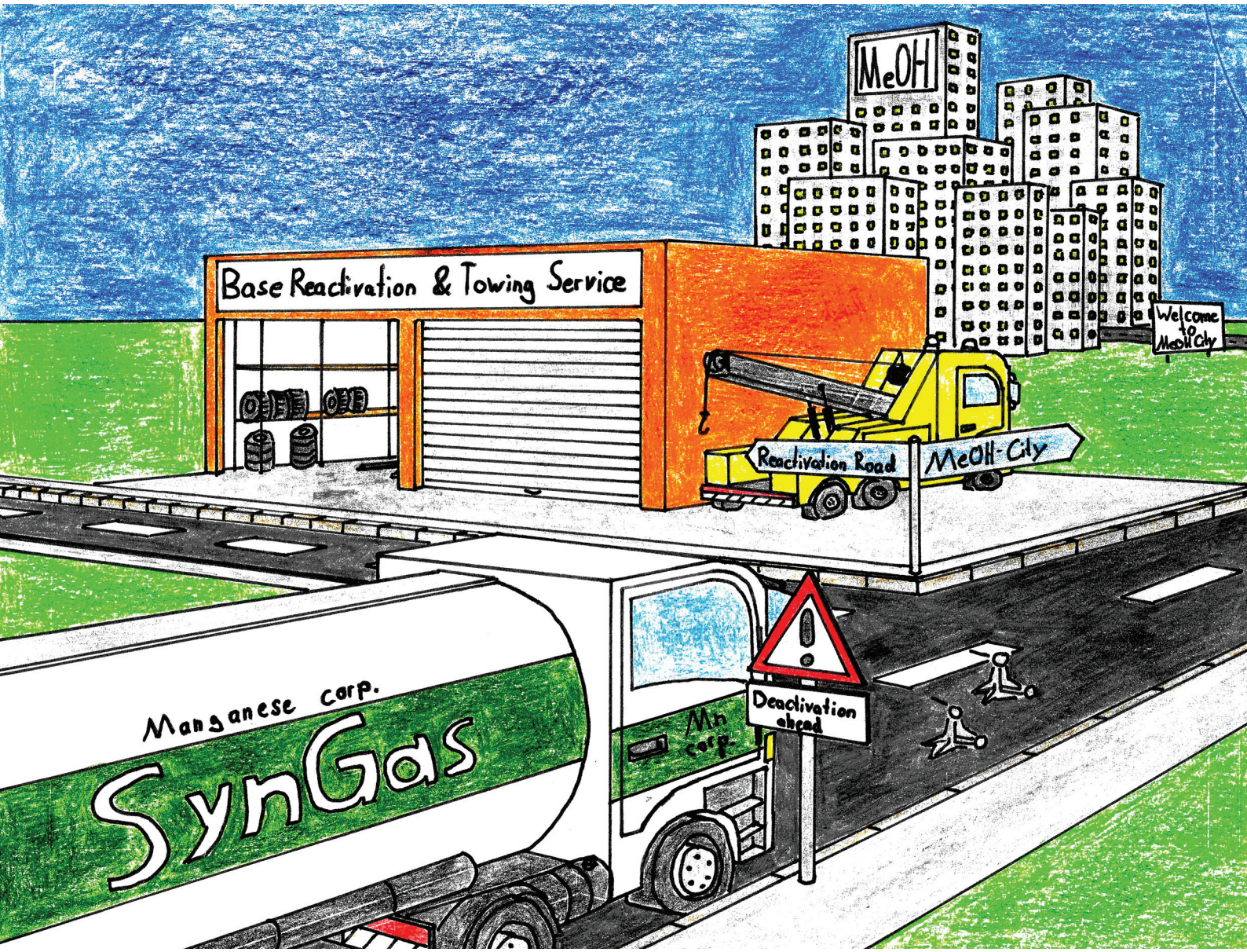

ISSN 1463-9262

ROYAL SOCIETY OF CHEMISTRY

PAPER

Walter Leitner, Andreas J. Vorholt *et al.*
Continuously operated liquid-phase methanol synthesis uncovering the de-/activation pathways of a molecular manganese catalyst system

Green Chemistry

PAPER

View Article Online
View Journal | View Issue

Cite this: *Green Chem.*, 2026, **28**, 3549

Continuously operated liquid-phase methanol synthesis uncovering the de-/activation pathways of a molecular manganese catalyst system

Sebastian Stahl,[a,b] Lisa Steinwachs,[a,b] Walter Leitner *[a,b] and Andreas J. Vorholt *[a]

Received 24th September 2025,
Accepted 7th November 2025

DOI: 10.1039/d5gc05072c

rsc.li/greenchem

Homogeneously catalyzed synthesis of methanol from synthesis gas is achieved under continuous operation with product separation and catalyst recycling *via* simple flash distillation. A high-boiling alcohol is used as the solvent and stationary phase to immobilize the molecular manganese complex catalyzing the alcohol-assisted methanol synthesis. Detailed studies on the robustness of the system revealed high stability of the organometallic framework of the catalyst and identified the base co-catalyst as the limiting factor. Etherification of the alcoholate base through reaction with the formate ester intermediates was found to lead to its chemical depletion. This results in the accumulation of a formate complex as a dormant species that hinders catalytic turnover. This mechanistic insight into the fundamental (de-)activation phenomena aided the development of an optimal base-dosing strategy and temperature optimization as key levers to achieve long-term stable catalytic performance. Stable catalyst activity was retained over 50 h of operation, resulting in a total turnover number (TTON) of 16 190 mol MeOH per mol Mn.

Green foundation

1. Methanol is considered a pivotal molecular vector for the sustainable transformation of the chemical industry and energy value chain. This work presents the first publication on continuous methanol production from synthesis gas using a molecular catalyst with the Earth-abundant metal manganese under mild conditions. With the proven tolerance to the intermittency of renewable energy supply, it holds great potential for the production of green methanol.
2. We uncovered the molecular (de-)activation steps of the catalyst, which enabled a significant prolongation of its lifetime to the demonstrated 50 h of operation and beyond by the simple addition of small amounts of the base activator (<0.4 mol%). Manganese leaching into the product phase remains below the detection limit.
3. A deeper understanding of the factors influencing the etherification side reaction can suppress catalyst deactivation and thus reduce the amount of base addition needed.

1 Introduction

"Green" methanol is considered an essential bridge between renewable energy and a sustainable chemical and energy supply chain.[1–8] Methanol is already today one of the highest-volume base chemicals and an important C1 building block. It is used as a raw material for organic transformations such as the production of formaldehyde or acetic acid and can be transformed *via* methanol-to-olefin and methanol-to-gasoline processes into aliphatic and aromatic hydrocarbons.[9–13] Methanol is an attractive substitute fuel in hard-to-electrify sectors such as heavy-duty transportation and the shipping industry, as documented by recent investments from major shipping companies in methanol-powered vessels.[14–17] Additionally, methanol is not only a promising hydrogen carrier through reforming,[18–20] but can also be decomposed to 2 H_2 and CO,[21] making use of its carbon content, as we[22] and others[23] have recently shown for hydroformylation.

Synthesis gas, *i.e.*, the mixture of H_2/CO, obtained from CO_2 through reverse water–gas shift or electrocatalytically, from biomass, or from waste recycling, offers a non-fossil feedstock basis for methanol production.[24–26] While the heterogeneously catalyzed methanol synthesis from synthesis gas operating at high temperatures (>200 °C) is well established in fossil-based technology,[27–30] the use of homogeneous catalysis for this transformation has only started to see rising interest in recent years. The expected lower operating temperatures result in higher one-through conversion of CO due to favorable

[a]*Max Planck Institute for Chemical Energy Conversion, Stiftstraße 34–36, 45470 Mülheim an der Ruhr, Germany. E-mail: walter.leitner@cec.mpg.de, andreas-j.vorholt@cec.mpg.de*
[b]*Institute for Technical and Macromolecular Chemistry, RWTH Aachen University, Worringerweg 2, 52074 Aachen, Germany*

thermodynamics in the liquid phase, as has already been demonstrated at scale for slurry-phase processes using solid catalysts.[31,32] Together with the flexibility of organometallic catalyst design, such processes may hold unexplored potential for integration with decentralized renewable energy and feedstock supply.

The synthesis of methanol from syngas using organometallic complexes does not occur *via* direct "CO hydrogenation" as the insertion of CO into metal–hydride bonds is energetically strongly uphill and therefore cannot constitute an elementary step in a catalytic cycle. Recent advances to circumvent this obstacle include the seminal work of the groups of Prakash[33] and Beller.[34] They used amines as co-reagents to activate CO in the form of formamides which subsequently enter a hydrogenation cycle catalyzed by a manganese–pincer complex comprising a MACHO-type ligand (**I**). The limitations of these systems such as incomplete formamide conversion and the formation of trace amounts of *N*-methylated side-products could be overcome by the development of alcohol-assisted CO hydrogenation involving formate esters as the reactive intermediates.[35,36] A first attempt to demonstrate the liquid phase Mn-catalyzed synthesis of methanol from syngas on a pilot scale was recently implemented.[37–39] In our work, we focus on the fundamental steps of activation and deactivation within the complex reaction network of the catalytic system as a basis for rational optimization strategies under continuous operation (Fig. 1).

In previous work (Fig. 1),[35] we directly confirmed that alcohol-assisted CO hydrogenation occurs *via* formate esters as intermediates formed *in situ* from the alcohol co-reagent and a catalytic amount of base. The formate group is then hydrogenated in two consecutive steps to methanol, liberating the alcohol co-reagent again for another catalytic turnover. It was also shown that methanol itself can act as the co-reagent, leading to "self-breeding" of the product alcohol.[35] In order to overcome the inherent challenges of homogeneous catalysis such as product separation and catalyst recycling, we recently further developed this catalytic system by introducing long-chain alcohols such as 1-dodecanol. In addition to their role as solvents, they simultaneously act as co-reagents by activating CO through the formation of reactive formate ester intermediates (Fig. 1).[40] The high boiling-point difference and the absence of azeotrope formation between the solvent and product alcohols facilitate product isolation *via* distillation. This enabled successful batch-wise recycling of the catalyst. Through the recycling, we discovered Brønsted base deactivation as a cause for activity deterioration over time.

In this study, we aimed to gain more insights into the robustness of the approach, catalyst stability, and potential deactivation pathways by transferring this recyclable catalytic system to continuous operation. As extensive optimization of the reaction parameters towards high catalytic performance has been conducted in our previous study, this is not a focus of the present work.[40] The ultimate goal is rather to understand the productive as well as the deactivation pathways in order to assess the potential of this catalytic system for the production of "green" methanol in conjunction with renewable energy sources.

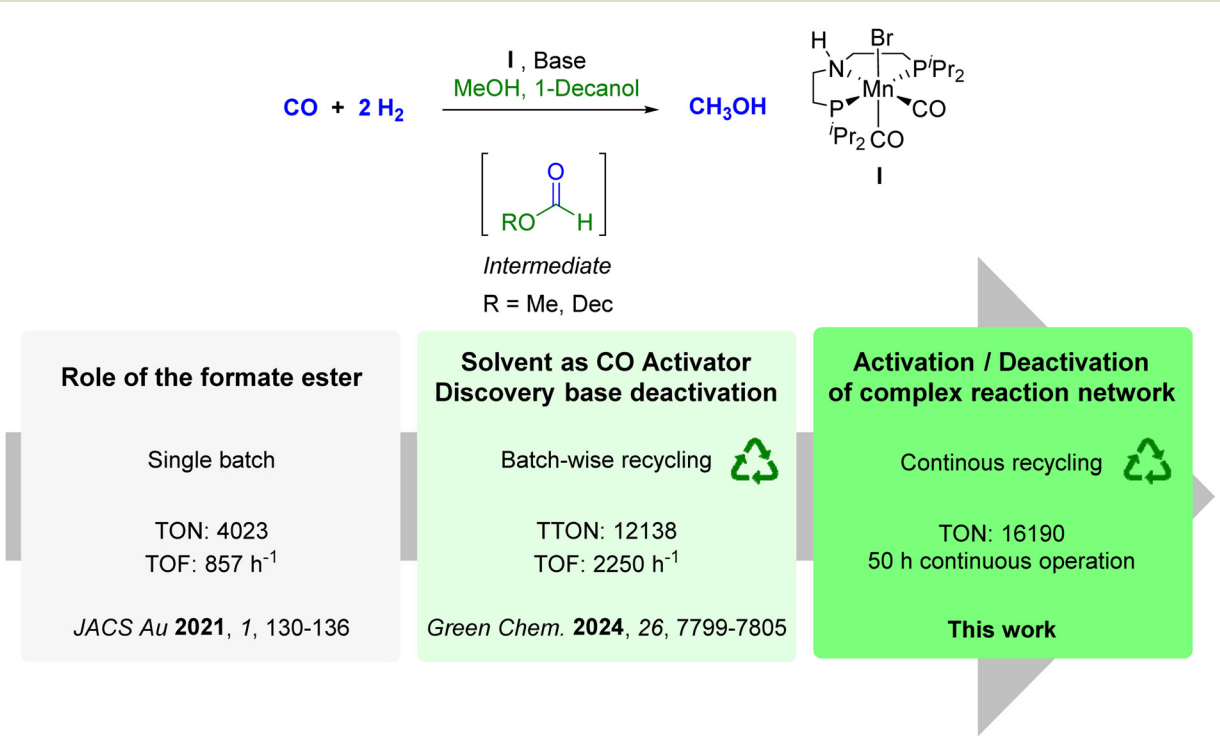

Fig. 1 Development of alcohol-assisted carbon monoxide hydrogenation to methanol with manganese pincer catalyst **I** from mechanistic understanding to continuous operation.[35,40]

2 Results and discussion

The catalytic system chosen for the continuously operated miniplant in this study was based on the components established in our previous work. The system comprises the molecular manganese complex $[Mn(CO)_2Br[HN(C_2H_4P^iPr_2)_2]]$ (**I**, Fig. 1), NaOMe as an activator for the catalyst[41] and as a base for formate ester formation, and a high-boiling alcohol solvent.[40] NaOMe exhibited similar performance to stronger bases such as NaO^{t}Bu in our earlier work. It simplifies the reaction system through minimizing the count of alcohol components in the reaction mixture, facilitating methanol separation and characterization of catalytic species. In order to avoid possible solidification of the solvent alcohol, which also acts as a co-reagent to activate CO, in the recycling stream, 1-decanol was employed instead of the previously used 1-dodecanol.[40] This ensures a constant liquid flow in all parts of the setup while maintaining the boiling point difference relative to methanol as high as possible. Control experiments confirmed similar reactivity for both solvents within experimental error (SI, Table S1). Reactions were performed using **I** (1.36 mmol L^{-1}) and NaOMe (68 mmol L^{-1}, 50 eq. with respect to **I**) in a total liquid volume of 220 mL of 1-decanol containing initially 5 Vol% methanol as a primer that showed an accelerating effect in our previous study.[40] While the CO hydrogenation can proceed *via* the formate ester intermediates of the solvent (decyl formate) or the product (methyl formate), the latter is formed significantly faster, thus explaining the accelerating effect of small initial methanol loadings. The dual role of the long-chain alcohol as a solvent and co-reagent provides higher operational flexibility as methanol production persists independently of the methanol loading, even in its complete absence.

The integrated reaction/separation set-up (Fig. 2) contains as the central part a stainless-steel high-pressure reactor (**1**, 300 mL) maintained at the reaction temperature and pressure and a stainless-steel flash-distillation unit (**2**, 160 ml) at the separation temperature and 2–3 bar pressure. The reactive gases CO and H_2 are constantly fed into the reactor at the desired ratio and pressure. The pressure inside the reactor is set using a back-pressure regulator (BPR) (30 or 60 bar). Once the pressure in the reactor exceeds the set value, the BPR releases liquid and/or gas until the pressure decreases below the set value. In this way, a constant liquid flow out of the reactor to the flash-distillation unit is achieved, splitting the 220 mL reaction medium into around 160 mL constantly present in the reactor and 60 mL in the separation and recycling loop. In the separator (**2**, Fig. 2), methanol is distilled from the liquid phase and condensed for product collection. The stationary liquid phase containing the catalyst and base, collected at the bottom part of the flash distillation, is fed back into the reactor, closing the recycling loop (further details on the setup can be found in the SI). The high syngas pressure in the reactor and the reduced temperature (73–77 °C) and mild overpressure (2–3 bar) in the separator ensure that the catalyst does not engage in the reverse dehydrogenation of methanol at any point in the continuous setup.[21] The reactive gases are used to ensure a constant flow out of the reactor in the depicted setup, thus resulting in a loss of a portion of the reactive gases. Therefore, stating conversion or yield figures is not meaningful, and rather molar amounts and TON are used. However, our previous study conducted in batch mode showed full conversion of CO under the employed conditions.[40]

The initial experiment was conducted at 150 °C and 30 bar with a CO to H_2 ratio of 1 : 5 over 30 h. Fig. 3 (left) illustrates

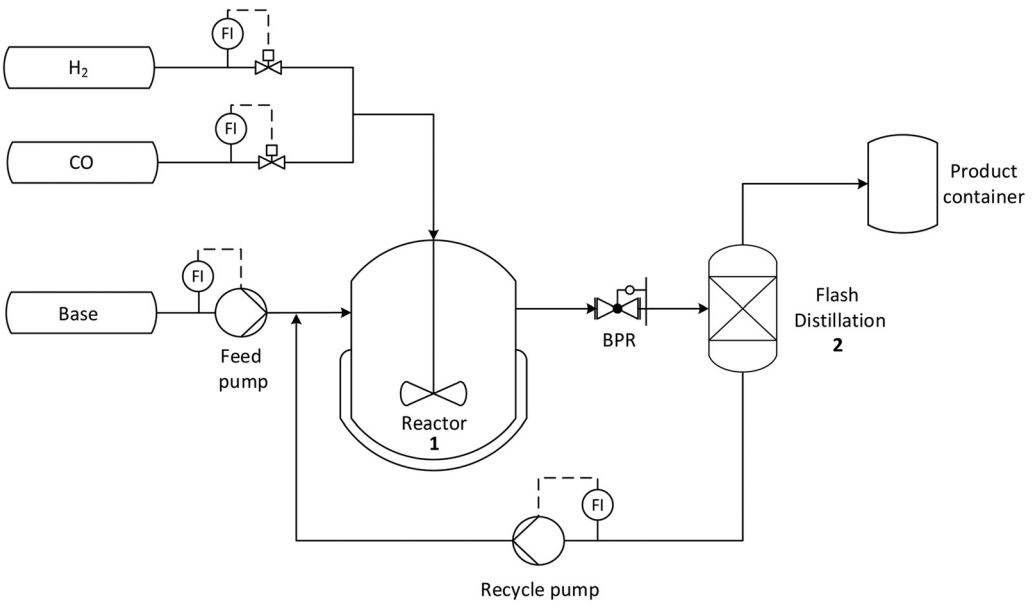

Fig. 2 Flow scheme of the reactor setup used in this study.

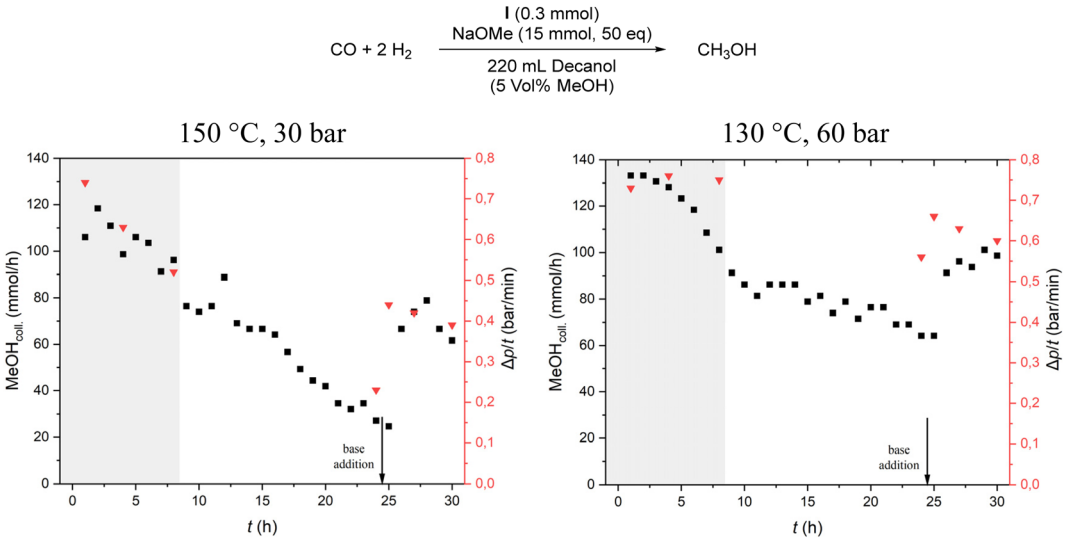

Fig. 3 CO hydrogenation to methanol with continuous product separation and catalyst recycling in the miniplant setup. Left: 150 °C and 30 bar. Right: 130 °C and 60 bar. Induction period for the removal of pre-charged methanol (grey). Reaction conditions: $[Mn(CO)_2Br[HN(C_2H_4P^iPr_2)_2]]$ catalyst precursor (0.3 mmol, 1.36 mmol L^{-1}), NaOMe as the base (15 mmol, 50 eq.), 220 mL of 5 vol% MeOH in 1-decanol, *p* at a 1 : 5 ratio of CO : H_2, *T*, 1000 rpm, and 30 h. Base addition: NaOMe (7.5 mmol, 25 eq.) in 10 mL MeOH.

the development of the collected methanol every hour. As changes in the catalytic activity only translate with a certain delay in the amount of collected methanol, we additionally measured the activity *via* synthesis gas consumption ($\Delta p/t$) in bar per min regularly. For this measurement, the gas feed is stopped, the reactor is isolated from the recycling loop and the pressure drop is recorded for 2 min. A constant decline in collected methanol can be observed over 24 h in this first experiment. An initial drop in collected methanol is expected as the pre-charged methanol is distilled in the first 6 to 8 hours of the experiment (Fig. 3, grey). However, since the activity constantly drops to around a third of its initial value and the collected methanol is not reaching a plateau, catalyst and/or base deactivation are the likely causes for this loss in activity.

In our previous work, we have discovered Brønsted base deactivation as a major cause for activity deterioration.[40] The addition of an additional 25 eq. of base in 10 mL methanol after 24 h increased the activity to only 60% of its initial value, followed again by a slow decline. This incomplete restoration of the activity upon base addition indicates additional deactivation of the catalyst under these conditions. The drop in collected methanol after base addition is more pronounced as the methanol added with the base (similar to the initially charged methanol) is also distilled off from the reaction mixture in the first following hours.

To decrease long-term deactivation of the catalyst, the influence of pressure and temperature was investigated. Doubling the pressure from 30 to 60 bar at a constant CO : H_2 ratio of 1 : 5 (Fig. S1) also doubles the initial activity of the reaction (0.74 *vs.* 1.52 bar per min), showcasing the high accelerating effect of the gas concentration in solution. However, the pressure shows no influence on the deactivation behavior as both reactions show a loss of 30% of its initial activity within the first 8 hours. A temperature decrease to 140 °C (Fig. S1) only slightly reduces activity deterioration while a further decrease to 130 °C (Fig. S1) results in constant activity over the initial 8 hours. This temperature decrease by 20 °C halved the initial activity compared to the reaction at high temperature and high pressure. This run at 130 °C with a pressure of 60 bar exhibits a starting activity comparable to the initial experiment at 150 °C and 30 bar. When comparing both runs over 30 h, the enhanced stability of the system at a lower temperature is clearly visible in the activity and product collection (Fig. 3). After the initial induction period (grey area) with the removal of the precharged methanol, only a minor decrease in collected methanol occurs. While the activity at 150 °C drops within 24 h to 30% of its initial value, it remains at 78% at 130 °C. The addition of a base in the latter restores the activity up to 90% of its starting value, followed again by a slow decline. Based on our earlier study, which includes a broad temperature variation (120 to 170 °C), a further temperature reduction is not meaningful as formate ester hydrogenation to methanol comes to an almost complete standstill at 120 °C.[40]

To understand the fundamental steps of catalyst activation and deactivation in this reaction network, inert NMR samples were collected from the continuous setup at several time points. At 150 °C already after 1 h, significant quantities of a free ligand species (blue) become visible in the ^{31}P-spectra and its concentration significantly increases over time (Fig. 4, left) as a sign of catalyst decomposition. Control experiments with the pincer ligand **LI** showed that it forms the carbonylated formamide species **LII** in the presence of a base and CO, giving rise to a doublet in the blue region (Scheme 1). As formamides have been reported as a method for CO activation for its hydrogenation to methanol, under catalytic conditions **LII** can be hydrogenated to methanol and **LI**.[33,34] This decoordination

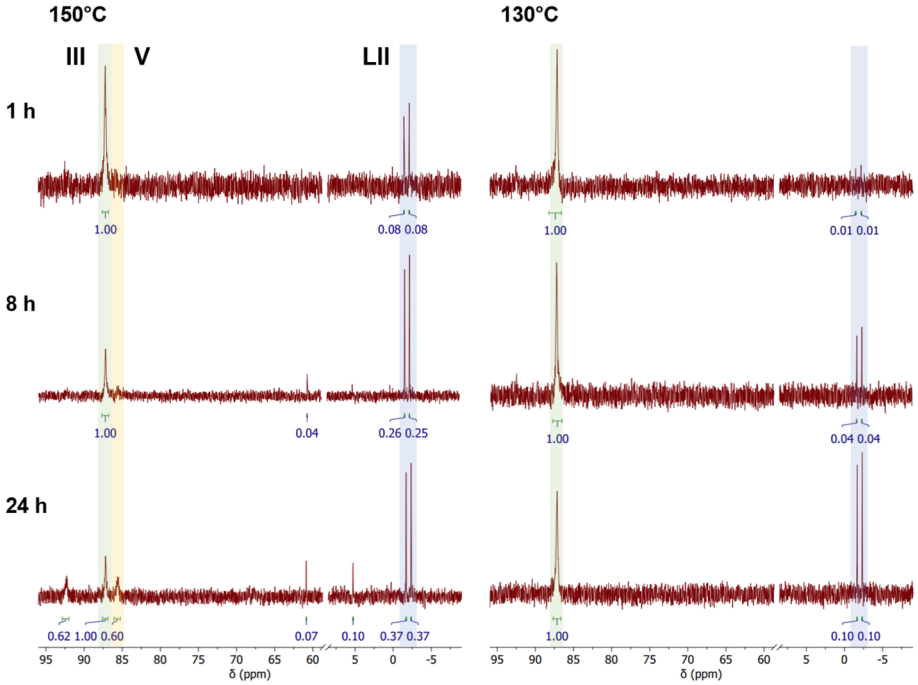

Fig. 4 ^{31}P-NMR (162 MHz, methanol) spectra of the reaction at 150 °C and 30 bar (left) and the reaction at 130 °C, 60 bar (right) after 1 h, 8 h and 24 h. δ = −1.8 (blue, free Ligand **LII**), 85.6 (yellow, dormant species **V**), 87.1 (green, active catalyst **III**), and 92.3 (deactivated species) ppm.

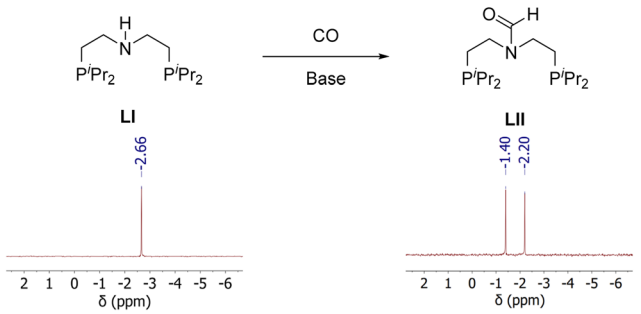

Scheme 1 Carbonylation of free ligand **LI** (δ = −2.66 ppm) to formamide **LII** (δ = −1.8 ppm, ^{31}P-NMR (162 MHz, methanol)).

and carbonylation of the ligand from the catalyst are significantly reduced at 130 °C while still slightly increasing over time.

Additional signs for catalyst deactivation are the significant formation of different, presumably manganese-coordinated species at 85.6 and 92.3 ppm, and consequently, a relative decline of catalytic resting state **III**. In contrast, at 130 °C (right), no signs of those species arise even after 24 h, reflecting the stabilized catalytic activity and methanol production.

While the species at 92.3 ppm presumably corresponds to an unknown thermal deactivation product, species **V** at 85.6 ppm was previously described in the literature as a formic-acid-coordinated complex.[42] **V** forms in the presence of formate, which stems from a side reaction described later in the manuscript, or CO_2 and H_2. We confirmed this species *via* control experiments in 20 mL autoclaves. Here, we used just enough base (2 eq.) to deprotonate/activate **I** and form **V** *via* the addition of CO_2 and H_2 (Fig. 5). The product of this reaction exhibits the same chemical shift at 85.6 ppm.

Subsequently, 50 eq. of base in 1 mL of methanol were added to one autoclave (top), and only methanol was added to the other (bottom). Both mixtures were then subjected to standard CO hydrogenation conditions. While the autoclave with an added base showed full conversion of CO to methanol and the formation of catalytic resting state **III**, without further base addition, the catalyst remains in dormant species **V** and no methanol was formed.

Therefore, the beneficial effect of base addition during the reaction goes beyond replacing the deactivated base to ensure the sufficient formation of the reactive formate ester intermediate. It also breaks dormant species **V** and rebuilds catalytic resting state **III** (Scheme 3).

This ability to tolerate small amounts of CO_2 through the addition of a base is of great importance for the industrial application of this system. It shows the opportunity to directly convert renewable CO streams from sources like CO_2 electrolysis that contain small amounts of CO_2 instead of relying on highly purified CO sources.[43,44]

This then leaves the questions of where the CO_2 or formate-forming species **V** originates as well as the cause for the Brønsted base deactivation. Small amounts of 1-methoxydecane detected in the reaction solution indicate etherification of the base and the solvent alcohol as the responsible side reaction. As etherification normally does not occur under basic conditions, control experiments were conducted to elucidate the roles of the catalyst and the formate esters

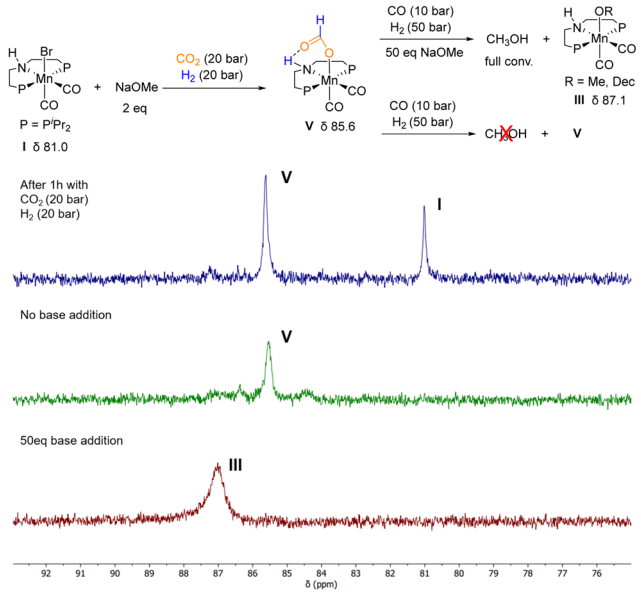

Fig. 5 Control experiment and ^{31}P-NMR (162 MHz, methanol) spectra showing the influence of base on the carboxylic resting state of catalyst **I**. Reaction conditions: $[Mn(CO)_2Br[HN(C_2H_4P^iPr_2)_2]]$ catalyst precursor (7 μmol, 1.36 mmol L^{-1}), NaOMe as the base (14 μmol), 5 mL of 5 vol% MeOH in 1-decanol, *p*, 130 °C, 800 rpm, 20 mL stainless steel autoclave, 1 h (first step) and 24 h (second step). Second step: NaOMe (0.35 mmol) in 1 mL of MeOH (top) or only 1 mL of MeOH (bottom) added at r.t. δ = 81.0 (pre-catalyst **I**), 85.6 (dormant species **V**), and 87.1 (catalytic resting state **III**) ppm.

(Scheme 2). The ether was also found in the absence of catalyst **I** (a). However, without CO and consequently without formate esters, no ether products were detected (b). This indicates that the etherification occurs between a nucleophilic alcoholate and a formate ester as the electrophile with formate as the leaving group. This hypothesis is supported by minor sodium formate crystals that can be found on the reactor walls after the reaction. To the best of our knowledge, this describes a novel umpolung procedure for converting alcohols into a formate ester electrophile with the use of a base and CO.

These insights together with the learnings from our previous work lead to a holistic picture of the complex reaction network of the catalytic system for alcohol-assisted carbon monoxide hydrogenation to methanol including the fundamental steps of activation and deactivation (Scheme 3).[35,40] In the presence of a base, **I** is deprotonated/activated to **II** which can cleave hydrogen heterolytically to form catalytically active complex **IV**. **II** cannot be detected in alcoholic media as it immediately forms catalytic resting state **III**. **IV** has been reported under catalytic conditions but cannot be detected in our pressureless offline NMR measurements.[41,45] **IV** cannot hydrogenate CO directly, so it has to be activated as a formate ester. This intermediate is hydro-

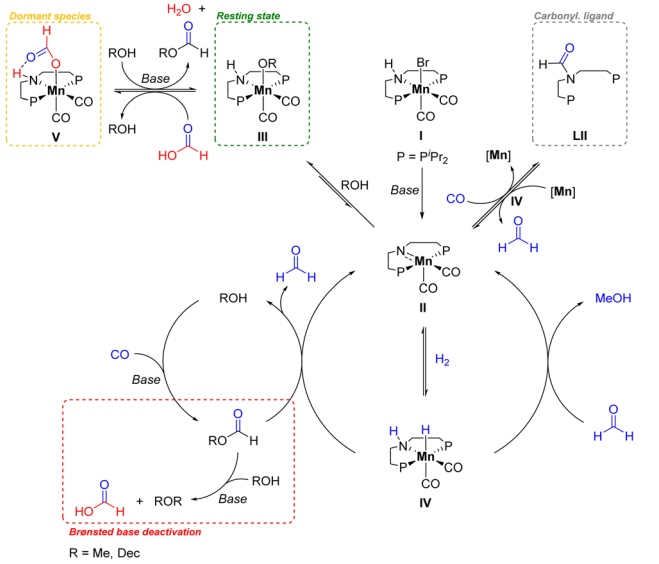

Scheme 3 Reaction network of alcohol-assisted carbon monoxide hydrogenation to methanol including activation and deactivation within the catalytic system.

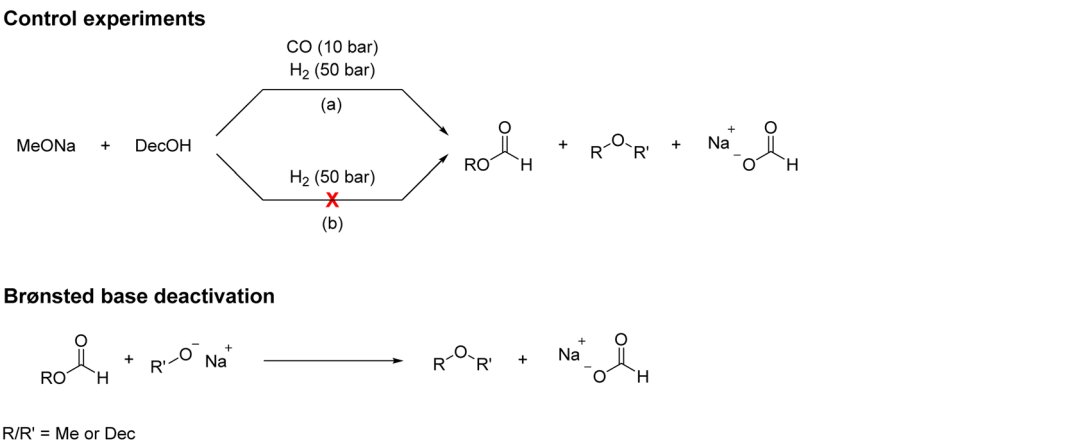

Scheme 2 Control experiments to probe the role of the catalyst and formate esters in the Brønsted base deactivation and the deactivation reaction. Reaction conditions (control experiments): NaOMe as the base (14 μmol), 5 mL of 1-decanol, *p*, 130 °C, 800 rpm, 16 h, and 20 mL stainless-steel autoclave.

genated by **IV** in the first cycle to formaldehyde, which is in the second cycle hydrogenated again by **IV** to methanol. Detection of this formaldehyde intermediate is impeded by its lower hydrogenation activation barrier compared to methyl formate.[36,46] These hydrogenation steps occur *via* the widely inferred metal–ligand cooperation (MLC) mechanism.[41,47–49] As an undesired side reaction, the reactive formate ester intermediate can undergo etherification with the alcoholate base with formate as the leaving group. This decreases the concentration of the alcoholate base necessary for CO activation.

Additionally, the formed formate can coordinate to **III**, forming dormant species **IV** that can be brought back into the catalytic cycle by esterification of the coordinated formate with the alcoholate base to rebuild **III** and the formate ester intermediate. A further deactivation pathway is the cleavage of the pincer ligand from the manganese complex. So far, it remains unknown which Mn species is the starting point for this ligand cleavage. We were able to detect it as its formamide species **LII**. Free ligand **LI** can be rebuilt through the hydrogenation of **LII**, additionally yielding formaldehyde.[33,34]

Aided by these insights into the molecular activation and deactivation phenomena, we aimed for a more stable long-term performance of the catalytic system. At the cost of slightly reduced activity, the initially charged base equivalents were reduced to 25 together with a more frequent addition of 12.5 eq. every 12 h. This results in a lower and more constant base concentration, decreasing etherification, which causes Brønsted base deactivation, and thus prohibiting accumulation of dormant species **V**. Additionally, the CO : H_2 ratio was changed to 1 : 8. In our previous study, we have shown the accelerating effect of a higher H_2 excess,[40] and a test reaction confirms this with an enhancement of the initial activity from 0.74 bar per min (1 : 5) to 0.87 bar per min (1 : 8). Employing these conditions, stable activity was achieved over 50 h (Fig. 6). The initial activity stayed constant at 0.74 bar per min compared to the previous experiment at 130 °C; thus, the de- and accelerating effects of reduced base and higher H_2 excess appear to cancel each other out. The drop in activity after 32 h is caused by the addition of 25 ml of 1-decanol, which was required to compensate for the loss of material through sample taking at various points during the reaction and is not a sign of deactivation. This addition dilutes the catalyst phase, thus reducing the activity that again remained constant after the addition. This enhanced stability is also supported by NMR data, which show no signs of deactivated catalyst species over the entire reaction time with only a minor constant portion of free ligand species **LII** (Fig. 6; more details in the SI, Fig. S2). Also, the hourly amount of the collected methanol was significantly stabilized after the induction phase, where the pre-charged methanol is distilled off (grey). The small increases after base addition are caused by the 4 mL of methanol added every 12 h to dissolve the base. Over the 50 h reaction time, a total methanol amount of 153.7 g (4.80 mol) was produced, corresponding to a TTON of 161 90 and a space–time yield of 10.2 g lh^{-1}. Despite the three base additions, the total base amount remains minimal, corresponding to

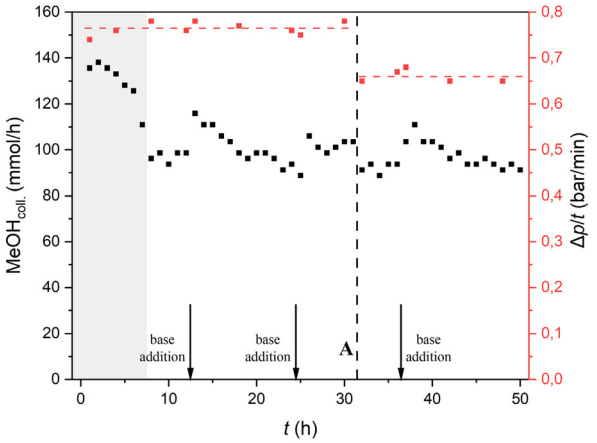

	1 h	12 h	24 h	36 h	48 h
III (87.1 ppm)	1.00	1.00	1.00	1.00	1.00
Deactivated species (85.6 V and 92.3 ppm)	-	-	-	-	-
LII (-1.8 ppm)	-	0.03	0.05	0.08	0.05

Fig. 6 Long-term CO hydrogenation to methanol with continuous product separation and catalyst recycling (top). Induction period for the removal of pre-charged methanol (grey). ^{31}P-NMR integral values for catalyst **III**, deactivated species (including **V**) and free ligand species **LII**. Reaction conditions: [$Mn(CO)_2Br[HN(C_2H_4P^iPr_2)_2]$] catalyst precursor (0.3 mmol, 1.36 mmol L^{-1}), NaOMe as the base (7.5 mmol, 25 eq.), 220 mL of 5 Vol% MeOH in 1-decanol, 60 bar at a 1 : 8 ratio of CO : H_2, 130 °C, 1000 rpm, and 50 h. Base addition: NaOMe (3.75 mmol, 12.5 eq.) in 4 mL of MeOH. **A**: Addition of 25 mL of 1-decanol.

<0.4 mol% of the produced methanol (a TON of 259 for the base). Catalyst leaching into the product phase with this setup was negligible. Manganese leaching stayed below the detection limit, and phosphorus (ligand) leaching accumulated to only <1 mg over the whole reaction time. Minor amounts of the solvent 1-decanol leached into the product phase but remained <1 wt% for every experiment shown. Further details on the produced methanol, TON and leaching for all experiments can be found in the SI.

To achieve compatibility of this catalytic system with renewable energy production, tolerance to the impacts of an intermittent, fluctuating power supply is necessary. We therefore tested the response of the catalytic system to the temporary absence of CO, H_2 and reactor heating (see the SI for further details). The absence of either one of the reactive gases shuts down the catalytic activity completely as expected. However, after turning on their supply once again, the activity reaches its previous level quickly. The same high tolerance was observed when the reaction solution was cooled to 50 °C and heated again to the reaction temperature of 130 °C over 5 cycles.

3 Conclusion

In conclusion, our previously developed catalytic system for the alcohol-assisted liquid-phase hydrogenation of carbon monoxide to methanol was successfully transferred to continuous

operation. This enabled in-depth studies of the complex reaction network, unveiling the fundamental steps of activation and deactivation within the catalytic system. Etherification of the intermediate formate esters with the base alcoholate was uncovered as the key side reaction. This causes Brønsted base deactivation and the formation of a formate-coordinated dormant species. The importance of the base, besides activating CO, to break up these catalyst dormant species was uncovered. These mechanistic insights aided rational optimization of the operating parameters. A temperature reduction to 130 °C and a base-dosing strategy improved the long-term stability substantially. 50 h of steady operation were achieved using simple flash distillation for product separation and catalyst recycling, yielding a TTON of 16 190. Additionally, the stability of the catalytic system towards fluctuating process conditions and CO_2 impurities was confirmed. This high stability and flexibility showcase the great potential of this homogeneously catalyzed methanol production under mild conditions in conjunction with the intermittent power supply of renewable energy sources.

4 Experimental section

General considerations

All reactions were conducted under an argon inert-gas atmosphere unless stated otherwise, with argon supplied by AirLiquide (99.9999% purity). Air-sensitive chemicals were stored in a glovebox, and standard Schlenk techniques were applied. The solvents were degassed and purified using standard solvent purification systems and techniques and were stored over molecular sieves under argon. Chemicals were purchased from Sigma-Aldrich, Alfa-Aesar, abcr, and TCI Chemicals. All chemicals were used as obtained from the vendors and degassed before application in catalytic reactions. Carbon monoxide (99.997% purity) and hydrogen (99.999% purity) for catalytic reactions were obtained from AirLiquide.

GC measurements were conducted on a *Nexis GC-2030* purchased from Shimadzu with a flame ionization detector. *Rtx-5* columns of the company Restek with a length of 60 m, an inner diameter of 0.32 mm and a particle size of 1.5 μm were installed, and helium was used as a carrier gas. NMR measurements were carried out at ambient temperature using a *Bruker AVANCE NEO 400* spectrometer (^{1}H: 400 MHz, ^{31}P: 162 MHz) for the batch experiments. Chemical shifts were given in ppm, and the residual solvent signal of the deuterated solvent was referenced to trimethyl silane for ^{1}H NMR spectra and to phosphoric acid for ^{31}P NMR spectra. NMR samples were prepared under an inert gas atmosphere, unless stated otherwise.

XRF measurements were conducted on an *Xepos C* from Spectro. Samples were analyzed for manganese and phosphorus content.

Experimental procedure for the preparation of the Mn/pincer catalyst

The Mn/PNP (**I**) catalyst was prepared according to the procedure reported by Leitner *et al.*[41]

General procedure for experiments in 20 mL autoclave reactors

The reaction mixtures were prepared as stock solutions in a glovebox. The molecular complex $[Mn(CO)_2Br[HN(C_2H_4P^iPr_2)_2]]$ (1.36 mmol L^{-1}) and NaOMe (68 mmol L^{-1}) were added to a Schlenk tube and dissolved in 1-decanol or 1-dodecanol. A 20 ml stainless-steel autoclave (further details in the SI) was equipped with a stirring bar, closed, evacuated and purged with argon three times. The catalyst solution (1.5 mL for the solvent comparison and 5 ml for the control experiments) was added at room temperature through a ball valve under argon. The autoclave was pressurized *via* a needle valve with CO (10 bar) and/or H_2 (50 bar) and heated to the desired temperature and the reaction mixture was stirred for the desired time. After the reaction was completed, the autoclave was cooled to room temperature and slowly vented while stirring. 50 μL of mesitylene were added as an internal standard. The reaction mixture was analyzed by NMR spectroscopy. The control experiments were additionally analyzed by GCMS.

Analysis of the role of the alcoholate base on the resting states by NMR spectroscopy

The reaction mixture was prepared as a stock solution in a glovebox. The molecular complex $[Mn(CO)_2Br[HN(C_2H_4P^iPr_2)_2]]$ (1.36 mmol L^{-1}) and NaOMe (68 mmol L^{-1}) were added to a Schlenk tube and dissolved in 5 ml of 1-decanol with 5 vol% MeOH. A 20 ml stainless-steel autoclave (further details in the SI) was equipped with a stirring bar, closed, evacuated and purged with argon three times. The catalyst solution was added at room temperature through a ball valve under argon. The autoclave was pressurized *via* a needle valve with CO_2 (20 bar) and H_2 (20 bar) and heated to 130 °C, and the reaction mixture was stirred at 1000 rpm for 1 h. The autoclave was then cooled to room temperature and slowly vented while stirring. To remove the dissolved CO_2, the autoclave ball valve (**5**) was kept open under stirring while argon was flushed through the autoclave for 5 min. A sample was taken with a syringe and analyzed by NMR spectroscopy. To one autoclave, 1 mL of MeOH was added, and to another, 50 eq. of base in 1 ml MeOH was added through **5**. Both autoclaves were pressurized with CO (10 bar) and H_2 (50 bar) and heated to 130 °C, and the reaction mixture was stirred at 1000 rpm for 24 h. After the reaction time, the autoclaves were cooled to room temperature and slowly vented while stirring. 50 μL of mesitylene were added as an internal standard. The reaction mixture was analyzed by NMR spectroscopy.

General procedure for continuous experiments

The setup used in this study (further details in the SI) consists of a 300 mL stainless-steel reactor supplied by Parr Instrument Company that is connected to a product separation and recycling loop with a back-pressure regulator (BPR). The reactive gases CO and H_2 are fed constantly into the reactor. The feed rate (0.3 to 2.4 mol h^{-1}) and the ratio are controlled using a *Bronkhorst Mini CoriFlow* flowmeter. Liquids can be fed into the reactor under pressure using the feed pump. The pressure

inside the reactor is set using the BPR that is connected to a dip tube located in the middle of the reactor. Once the pressure in the reactor exceeds the set value, the BPR releases liquid and/or gas until the pressure decreases below the set value. This ensures a constant material flow into the recycling loop while maintaining a constant liquid level of 160 mL in the reactor. The pressure of the material released from the reactor is reduced after the BPR by expansion into a 300 mL stainless steel vessel before flowing into the flash distillation unit. This is a 160 mL stainless steel vessel filled with 3 mm glass tubes as column packaging for increased condensation surface. It is heated using a cryostat (*IKA* HBC 5 basic) with heating oil *via* copper coils. The vapor containing methanol and synthesis gas exits the vaporizer at the top through a *Bronkhorst Mini CoriFlow* flowmeter, and the methanol is condensed using dry ice and collected in a 50 mL glass burette. The hourly collection of methanol is monitored using a camera. The synthesis gas is then released into the off-gas. The remaining liquids collect at the bottom of the flash distillation unit and are pumped back into the reactor using the recycle pump at a rate of 180 mL h^{-1}. The pumps used are HPLC pumps supplied by Flusys (Type WADose-Lite-HP-40-SS-I-TU-C).

The reaction mixtures were prepared as stock solutions in a glovebox. The molecular complex $[Mn(CO)_2Br[HN(C_2H_4P^iPr_2)_2]]$ (1.36 mmol L^{-1}) and NaOMe (68 mmol L^{-1}) were added to a Schlenk tube and dissolved in 1-decanol with 5 vol% MeOH. The cryostat for the temperature control of the vaporizer was set to 112 °C, which corresponds to an internal temperature of 73–77 °C, 1 h prior to the reaction start. The reactor was purged with hydrogen three times before the reaction mixture was added *via* the feed pump over 10 min while stirring at 1000 rpm. At the same time, CO and H_2 were slowly added at the desired ratio, and the reactor was heated to the desired temperature. Once the reaction temperature and pressure were reached, the valve to the BPR was opened under a constant feed of the two reactive gases at the desired rate. After 5 min, the recycling pump was started. Samples of the catalyst phase were taken after the recycle pump and analyzed *via* NMR spectroscopy. At the end of the reaction, the gas feed was stopped, and the reactor was cooled using an ice bath to room temperature before the remaining synthesis gas was released. The collected methanol is analyzed *via* GC chromatography and XRF.

Conflicts of interest

The authors declare no conflict of interest.

Data availability

The data supporting this have been included as part of the supplementary information (SI). Supplementary information: additional graphics, detailed experimental procedures and analytical data. See DOI: https://doi.org/10.1039/d5gc05072c.

Acknowledgements

We gratefully acknowledge financial support from the Max Planck Society. The studies were performed as part of our activities in the framework of the "Fuel Science Center" funded by the Deutsche Forschungsgemeinschaft (DFG), German Research Foundation under Germany's Excellence Strategy – Cluster of Excellence 2186 "The Fuel Science Center" – ID: 390919832. We also want to acknowledge the support from FUNCAT. Open Access funding enabled and organized by Projekt DEAL. Open Access funding provided by the Max Planck Society.

References

1 A. González-Garay, M. S. Frei, A. Al-Qahtani, C. Mondelli, G. Guillén-Gosálbez and J. Pérez-Ramírez, Plant-to-planet analysis of CO2-based methanol processes, *Energy Environ. Sci.*, 2019, **12**, 3425–3436.
2 R. Schlögl, Chemical Batteries with CO2, *Angew. Chem., Int. Ed.*, 2022, **61**, e202007397.
3 J. Artz, T. E. Müller, K. Thenert, J. Kleinekorte, R. Meys, A. Sternberg, A. Bardow and W. Leitner, Sustainable Conversion of Carbon Dioxide: An Integrated Review of Catalysis and Life Cycle Assessment, *Chem. Rev.*, 2018, **118**, 434–504.
4 F. Sha, Z. Han, S. Tang, J. Wang and C. Li, Hydrogenation of Carbon Dioxide to Methanol over Non–Cu-based Heterogeneous Catalysts, *ChemSusChem*, 2020, **13**, 6160–6181.
5 J. Zhong, X. Yang, Z. Wu, B. Liang, Y. Huang and T. Zhang, State of the art and perspectives in heterogeneous catalysis of CO2 hydrogenation to methanol, *Chem. Soc. Rev.*, 2020, **49**, 1385–1413.
6 M. Bertau, H. Offermanns, L. Plass, F. Schmidt and H.-J. Wernicke, *Methanol: The Basic Chemical and Energy Feedstock of the Future*, Springer-Verlag, Berlin, Heidelberg, 2014.
7 G. A. Olah, A. Goeppert and G. K. S. Prakash, *Beyond Oil and Gas: The Methanol Economy*, Wiley-VCH Verlag GmbH & Co. KGaA, Weinheim, 2018.
8 A. Sonthalia, N. Kumar, M. Tomar, V. Edwin Geo, S. Thiyagarajan and A. Pugazhendhi, Moving ahead from hydrogen to methanol economy: scope and challenges, *Clean Technol. Environ. Policy*, 2023, **25**, 551–575.
9 H. I. Mahdi, N. N. Ramlee, D. H. d. S. Santos, D. A. Giannakoudakis, L. H. de Oliveira, R. Selvasembian, N. I. W. Azelee, A. Bazargan and L. Meili, Formaldehyde production using methanol and heterogeneous solid catalysts: A comprehensive review, *Mol. Catal.*, 2023, **537**, 112944.
10 G. J. Sunley and D. J. Watson, High productivity methanol carbonylation catalysis using iridium: The Cativa™ process for the manufacture of acetic acid, *Catal. Today*, 2000, **58**, 293–307.

11 M. Yang, D. Fan, Y. Wei, P. Tian and Z. Liu, Recent Progress in Methanol-to-Olefins (MTO) Catalysts, *Adv. Mater.*, 2019, **31**, 1902181.
12 K. Natte, H. Neumann, M. Beller and R. V. Jagadeesh, Transition-Metal-Catalyzed Utilization of Methanol as a C1 Source in Organic Synthesis, *Angew. Chem., Int. Ed.*, 2017, **56**, 6384–6394.
13 V. Dieterich, A. Buttler, A. Hanel, H. Spliethoff and S. Fendt, Power-to-liquid via synthesis of methanol, DME or Fischer–Tropsch-fuels: a review, *Energy Environ. Sci.*, 2020, **13**, 3207–3252.
14 S. Simon Araya, V. Liso, X. Cui, N. Li, J. Zhu, S. L. Sahlin, S. H. Jensen, M. P. Nielsen and S. K. Kær, A Review of The Methanol Economy: The Fuel Cell Route, *Energies*, 2020, **13**, 596.
15 M. Svanberg, J. Ellis, J. Lundgren and I. Landälv, Renewable methanol as a fuel for the shipping industry, *Renewable Sustainable Energy Rev.*, 2018, **94**, 1217–1228.
16 A. P. Moller-Maersk, *Maersk to deploy first large methanol-enabled vessel on Asia - Europe trade lane*, 2024, https://www.maersk.com/news/articles/2023/12/07/maersk-to-deploy-first-large-methanol-enabled-vessel-on-asia-europe-trade-lane (accessed 2025 20.07.).
17 A. G. Hapag-Lloyd, *Hapag-Lloyd concludes long-term offtake agreement for green methanol*, 2024, https://www.hapag-lloyd.com/en/company/press/releases/2024/11/hapag-lloyd-concludes-long-term-offtake-agreement-for-green-meth.html (accessed 2025 20.07.).
18 M. Nielsen, E. Alberico, W. Baumann, H.-J. Drexler, H. Junge, S. Gladiali and M. Beller, Low-temperature aqueous-phase methanol dehydrogenation to hydrogen and carbon dioxide, *Nature*, 2013, **495**, 85–89.
19 H. V. M. Hamelers, O. Schaetzle, J. M. Paz-García, P. M. Biesheuvel and C. J. N. Buisman, Harvesting Energy from CO2 Emissions, *Environ. Sci. Technol. Lett.*, 2014, **1**, 31–35.
20 G. Garcia, E. Arriola, W.-H. Chen and M. D. De Luna, A comprehensive review of hydrogen production from methanol thermochemical conversion for sustainability, *Energy*, 2021, **217**, 119384.
21 A. Kaithal, B. Chatterjee, C. Werlé and W. Leitner, Acceptorless Dehydrogenation of Methanol to Carbon Monoxide and Hydrogen using Molecular Catalysts, *Angew. Chem., Int. Ed.*, 2021, **60**, 26500–26505.
22 S. Stahl, J. T. Vossen, S. Popp, W. Leitner and A. J. Vorholt, Methanolation of Olefins: Low-Pressure Synthesis of Alcohols by the Formal Addition of Methanol to Olefins, *Angew. Chem., Int. Ed.*, 2025, **64**, e202418984.
23 A. Bonde, J. B. Jakobsen, A. Ahrens, W. Huang, R. Jackstell, M. Beller and T. Skrydstrup, Integrating hydroformylations with methanol-to-syngas reforming, *Chem*, 2025, **11**, 102396.
24 S. R. Foit, I. C. Vinke, L. G. J. de Haart and R.-A. Eichel, Power-to-Syngas: An Enabling Technology for the Transition of the Energy System?, *Angew. Chem., Int. Ed.*, 2017, **56**, 5402–5411.
25 R. M. Bown, M. Joyce, Q. Zhang, T. R. Reina and M. S. Duyar, Identifying Commercial Opportunities for the Reverse Water Gas Shift Reaction, *Energy Technol.*, 2021, **9**, 2100554.
26 H. O. LeClerc, H. C. Erythropel, A. Backhaus, D. S. Lee, D. R. Judd, M. M. Paulsen, M. Ishii, A. Long, L. Ratjen, G. G. Bertho, C. Deetman, Y. Du, M. K. M. Lane, P. V. Petrovic, A. T. Champlin, A. Bordet, N. Kaeffer, G. Kemper, J. B. Zimmerman, W. Leitner and P. T. Anastas, The CO2 Tree: The Potential for Carbon Dioxide Utilization Pathways, *ACS Sustainable Chem. Eng.*, 2025, **13**, 5–29.
27 L. C. Grabow and M. Mavrikakis, Mechanism of Methanol Synthesis on Cu through CO2 and CO Hydrogenation, *ACS Catal.*, 2011, **1**, 365–384.
28 M. Behrens, F. Studt, I. Kasatkin, S. Kühl, M. Hävecker, F. Abild-Pedersen, S. Zander, F. Girgsdies, P. Kurr, B.-L. Kniep, M. Tovar, R. W. Fischer, J. K. Nørskov and R. Schlögl, The Active Site of Methanol Synthesis over Cu/ZnO/Al_2O_3 Industrial Catalysts, *Science*, 2012, **336**, 893–897.
29 K. C. Waugh, Methanol Synthesis, *Catal. Lett.*, 2012, **142**, 1153–1166.
30 Y. Yang, C. A. Mims, D. H. Mei, C. H. F. Peden and C. T. Campbell, Mechanistic studies of methanol synthesis over Cu from CO/CO2/H2/H_2O mixtures: The source of C in methanol and the role of water, *J. Catal.*, 2013, **298**, 10–17.
31 E. C. Heydorn, B. W. Diamond and R. D. Lilly, Commercial-scale Demonstration of the Liquid Phase Methanol (Lpmeoh) Process, Air Products Liquid Phase Conversion Company, L.P., (US), United States, 2003.
32 P. Tyagi and V. Kumar, Present and Future Perspectives of Liquid-Phase Slurry Processes Involved in Methanol and Dimethyl Ether Synthesis Using Biomass-Derived Syngas, *Energy Fuels*, 2023, **37**, 3328–3354.
33 S. Kar, A. Goeppert and G. K. S. Prakash, Catalytic Homogeneous Hydrogenation of CO to Methanol via Formamide, *J. Am. Chem. Soc.*, 2019, **141**, 12518–12521.
34 P. Ryabchuk, K. Stier, K. Junge, M. P. Checinski and M. Beller, Molecularly Defined Manganese Catalyst for Low-Temperature Hydrogenation of Carbon Monoxide to Methanol, *J. Am. Chem. Soc.*, 2019, **141**, 16923–16929.
35 A. Kaithal, C. Werlé and W. Leitner, Alcohol-Assisted Hydrogenation of Carbon Monoxide to Methanol Using Molecular Manganese Catalysts, *JACS Au*, 2021, **1**, 130–136.
36 G. Neitzel, R. Razzaq, A. Spannenberg, K. Stier, M. P. Checinski, R. Jackstell and M. Beller, An Improved Manganese Pincer Catalyst for low Temperature Hydrogenation of Carbon Monoxide to Methanol, *ChemCatChem*, 2024, **16**, e202301053.
37 M. P. Checinski, M. Beller, P. Ryabchuk and K. Junge, *(CreativeQuantum GmbH, Leibnitz-Institut für Katalyse e.V.)*, WO2020136003A1, 2020.
38 C1 Green Chemicals AG, DBI-Gastechnologisches Institut gGmbH Freiberg, Fraunhofer UMSICHT, Fraunhofer IWES, TU Berlin, *Leuna* 100, 2023, https://www.leuna100.de/de (accessed 2025 20.07.).
39 M. P. Checinski, R. Clauss, A. Kaithal and L. Suntrup, *(C1 Green Chemicals AG)*, EP4488254A1, 2023.

40 S. Stahl, N. Wessel, A. J. Vorholt and W. Leitner, Liquid-phase hydrogenation of carbon monoxide to methanol using a recyclable manganese-based catalytic system, *Green Chem.*, 2024, **26**, 7799–7805.
41 A. Kaithal, M. Hölscher and W. Leitner, Catalytic Hydrogenation of Cyclic Carbonates using Manganese Complexes, *Angew. Chem., Int. Ed.*, 2018, **57**, 13449–13453.
42 D. A. Kuß, M. Hölscher and W. Leitner, Hydrogenation of CO2 to Methanol with Mn-PNP-Pincer Complexes in the Presence of Lewis Acids: the Formate Resting State Unleashed, *ChemCatChem*, 2021, **13**, 3319–3323.
43 C. W. Li and M. W. Kanan, CO2 Reduction at Low Overpotential on Cu Electrodes Resulting from the Reduction of Thick Cu2O Films, *J. Am. Chem. Soc.*, 2012, **134**, 7231–7234.
44 M. Liu, Y. Pang, B. Zhang, P. De Luna, O. Voznyy, J. Xu, X. Zheng, C. T. Dinh, F. Fan, C. Cao, F. P. G. de Arquer, T. S. Safaei, A. Mepham, A. Klinkova, E. Kumacheva, T. Filleter, D. Sinton, S. O. Kelley and E. H. Sargent, Enhanced electrocatalytic CO2 reduction via field-induced reagent concentration, *Nature*, 2016, **537**, 382–386.
45 S. Fu, Z. Shao, Y. Wang and Q. Liu, Manganese-Catalyzed Upgrading of Ethanol into 1-Butanol, *J. Am. Chem. Soc.*, 2017, **139**, 11941–11948.
46 D. A. Kuß, M. Hölscher and W. Leitner, Combined Computational and Experimental Investigation on the Mechanism of CO2 Hydrogenation to Methanol with Mn-PNP-Pincer Catalysts, *ACS Catal.*, 2022, **12**, 15310–15322.
47 S. Elangovan, C. Topf, S. Fischer, H. Jiao, A. Spannenberg, W. Baumann, R. Ludwig, K. Junge and M. Beller, Selective Catalytic Hydrogenations of Nitriles, Ketones, and Aldehydes by Well-Defined Manganese Pincer Complexes, *J. Am. Chem. Soc.*, 2016, **138**, 8809–8814.
48 Y. Wang, L. Zhu, Z. Shao, G. Li, Y. Lan and Q. Liu, Unmasking the Ligand Effect in Manganese-Catalyzed Hydrogenation: Mechanistic Insight and Catalytic Application, *J. Am. Chem. Soc.*, 2019, **141**, 17337–17349.
49 B. Chatterjee, W.-C. Chang, S. Jena and C. Werlé, Implementation of Cooperative Designs in Polarized Transition Metal Systems—Significance for Bond Activation and Catalysis, *ACS Catal.*, 2020, **10**, 14024–14055.